Supporting Information

Ma *et al*. 10.1073/pnas.0808868105

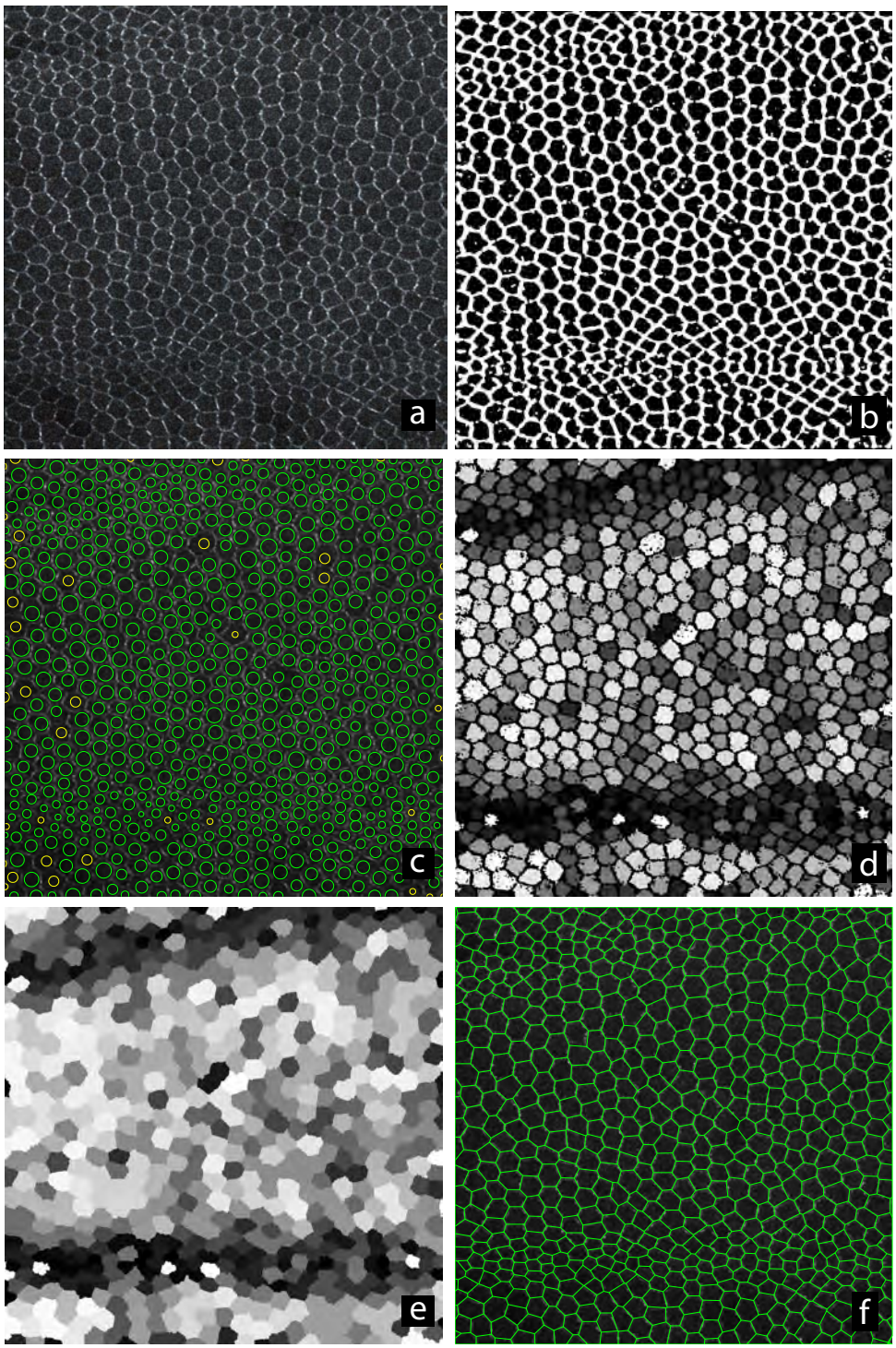

Fig. S1. Steps in the cell and edge analysis algorithm. (*a*) Original image of Dsh distribution 30 h after puparium formation (APF). (*b*) Separation of image into cell membrane (white) and interior (black) regions. (*c*) Individual cell detection, by fitting circles in the interior regions. (*d*) Expanded cell regions to approximate the shape of the detected cells. (*e*) Expanded cell regions to detect edge locations. (*f*) Cell edge locations overlaid on the original image.

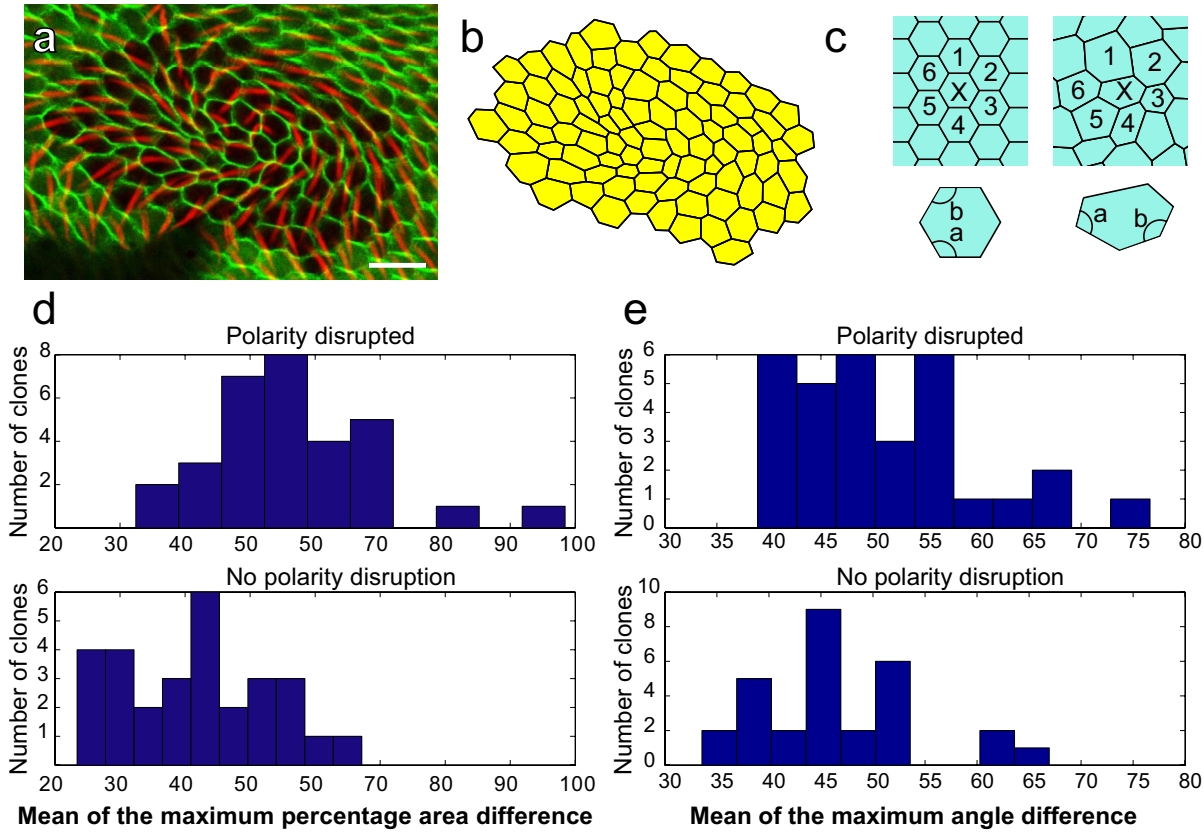

Fig. S2. Correlation between cell-shape irregularities and polarity disruption in fat clones. (*a*) A fat clone with polarity disruption and cell shape irregularities (phalloidin staining in red; cell junction marker ZCL1792 in green). (*b*) Representation of cell shapes from (*a*) captured with our image analysis program (Fig. S1). Only the clone cells are shown. (*c*) Illustrations of measures to quantify regularity of cell geometries: two measures were derived to quantify and compare geometric regularity. Mean of the maximum percentage area difference is given by

$$\frac{1}{N}\sum_{i=1}^{N}\frac{\max_j|A_i - A_j|}{A_i}$$

where N is the number of cells in the clone, A_i is the area of cell i, and j is an index over the cells neighboring cell i. The mean of the maximum angle difference is given by

$$\frac{1}{N}\sum_{i=1}^{N}\max_k \theta_{i,k} - \min_k \theta_{i,k}$$

where $\mu_{i,k}$ is the kth internal angle of cell i. Differences were determined by using a one-tailed Student's t test and assumed normal distributions ($r^2 = 0.05$). In a perfect hexagonal array (*Top Left*), the percent area difference between each cell X and its neighbors (cells 1–6) is zero; in irregular arrays, this value is greater than zero. Similarly, a perfect hexagonal cell has a maximum internal angle difference of zero (*Bottom Left*; $b - a = 0$); in irregular cells, the maximum internal angle difference is greater than zero (*Bottom Right*; $b - a > 0$). Histograms plotting the Mean of the maximum percentage area difference (*d*) and Mean of the maximum angle difference (*e*) for 31 fat clones that exhibit polarity disruptions (mean size: 1,105 microns^2, SD = 545), and for 28 fat clones that show wild-type polarity (mean size: 981 microns^2, SD = 459).

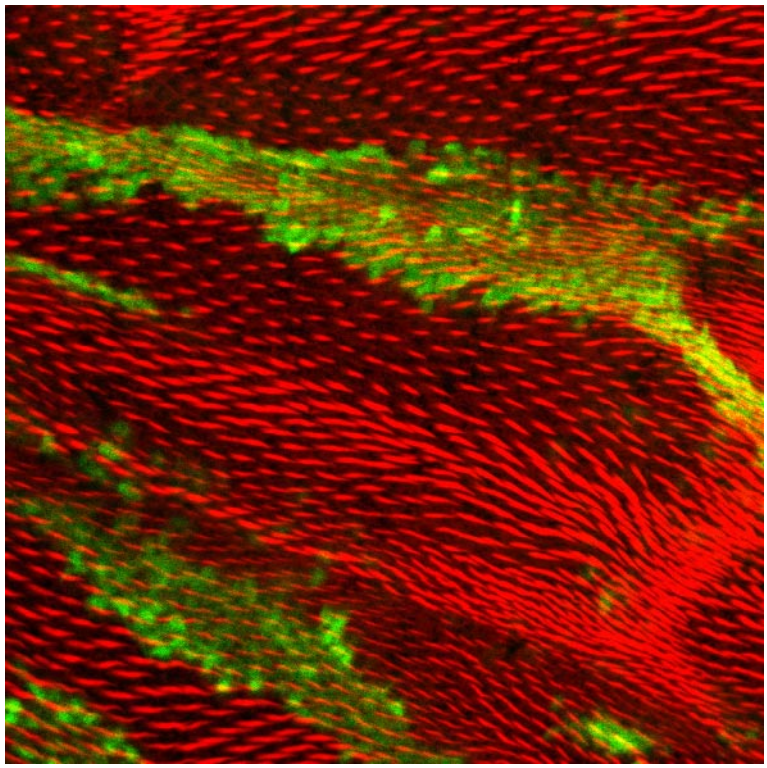

Fig. S3. PTEN mutant clones do not disrupt polarity. An image of PTEN mutant clones, marked by absence of GFP, stained at approximately 34-h APF with phalloidin (red) to show the orientation of prehairs. The polarity is not disrupted in the mutant clones.

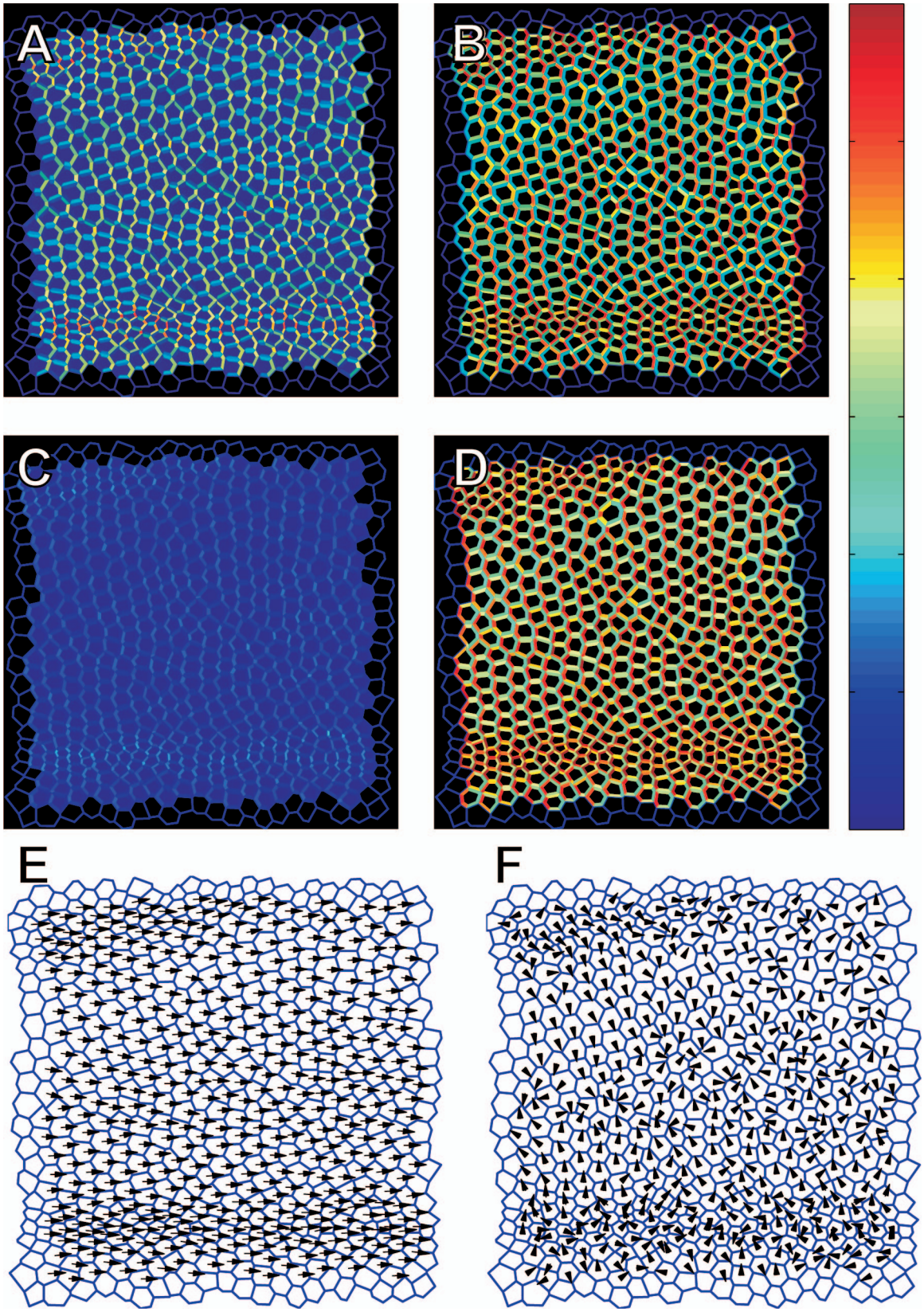

Fig. S4. Results from a mathematical model that simulates PCP implemented with real cell geometry. In all panels, the same field of cells is used. Cell geometry is extracted from an image of a 32 h APF wild-type pupal wing. (*A*–*D*). Near steady-state protein localization from a simulation of wild-type PCP signaling. Colored bar graph indicates the relative level of protein present at each cell boundary or cell interior: Dsh (*A*), Fz (*B*), Pk (*C*), and Vang (*D*). (*E*) Hair polarity derived from Dsh protein localization (*A*). Vector orientation represents the orientation of the hair, and vector length represents the amount of Dsh asymmetry within the cell. (*F*) Prediction of polarity in the same wing but in the absence of the global asymmetry input.

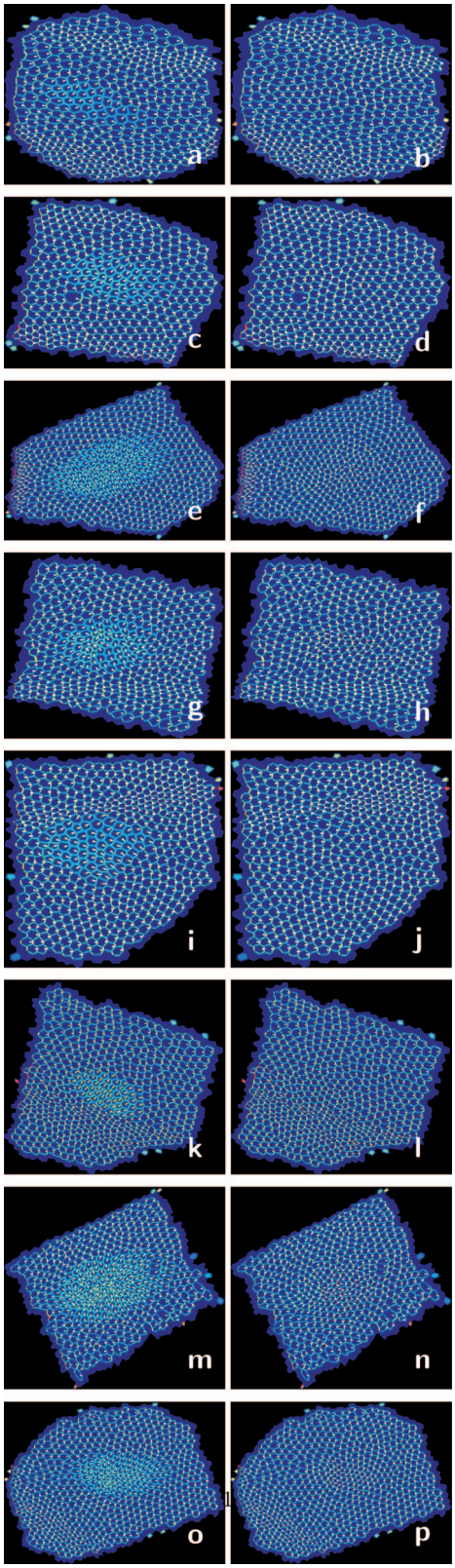

Fig. S5. Dsh distributions from simulated *fat* clones and surrounding regions. (*a*–*d*) Dsh distributions for simulated cases by using geometries extracted from fat clones showing normal polarity that were used to train the selected parameter set. (*a* and *c*) Simulated fat clones. (*b* and *d*) Simulated wild-type cells using the same geometry. (*e*–*h*) Dsh distributions for simulated cases using geometries extracted from fat clones showing perturbed polarity that were used to train the selected parameter set. (*e* and *g*) Simulated fat clones. (*f* and *h*) Simulated wild-type cells using the same geometry. (*i*–*l*) Dsh distributions for simulated cases using geometries extracted from fat clones showing normal polarity that were not used to train the selected parameter set. (*i* and *k*) Simulated fat clones. (*j* and *l*) Simulated wild-type cells using the same geometry. (*m*–*p*) Dsh distributions for simulated cases using geometries extracted from fat clones showing perturbed polarity that were not used to train the selected parameter set. (*m* and *o*) Simulated fat clones. (*n* and *p*) Simulated wild-type cells using the same geometry.

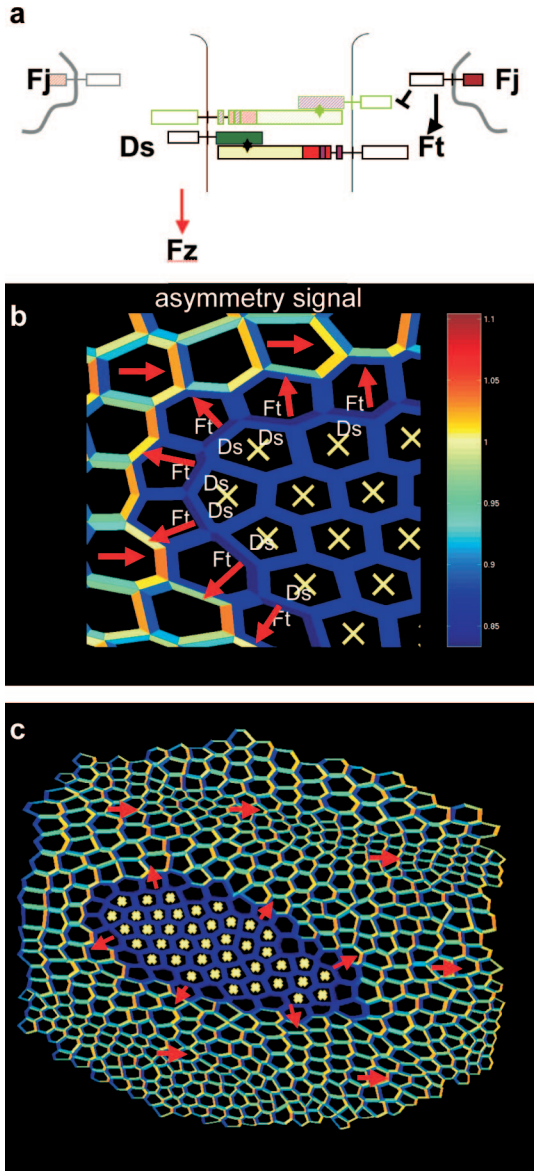

Fig. S6. Adjustment of the simulations to represent Ft-Ds nonautonomy near *fat* clone boundaries. (*a*) Ft-Ds heterodimers orient in 2 possible directions. Tissue gradients of Fj and Ds favor the accumulation of one orientation over the other. (*b* and *c*) Ds within ft clones accumulates selectively at interfaces with wild-type cells that express Ft. Ft within wild-type cells is therefore drawn to clone boundaries, altering the direction of the global directional signal in wild-type cells surrounding the clone.

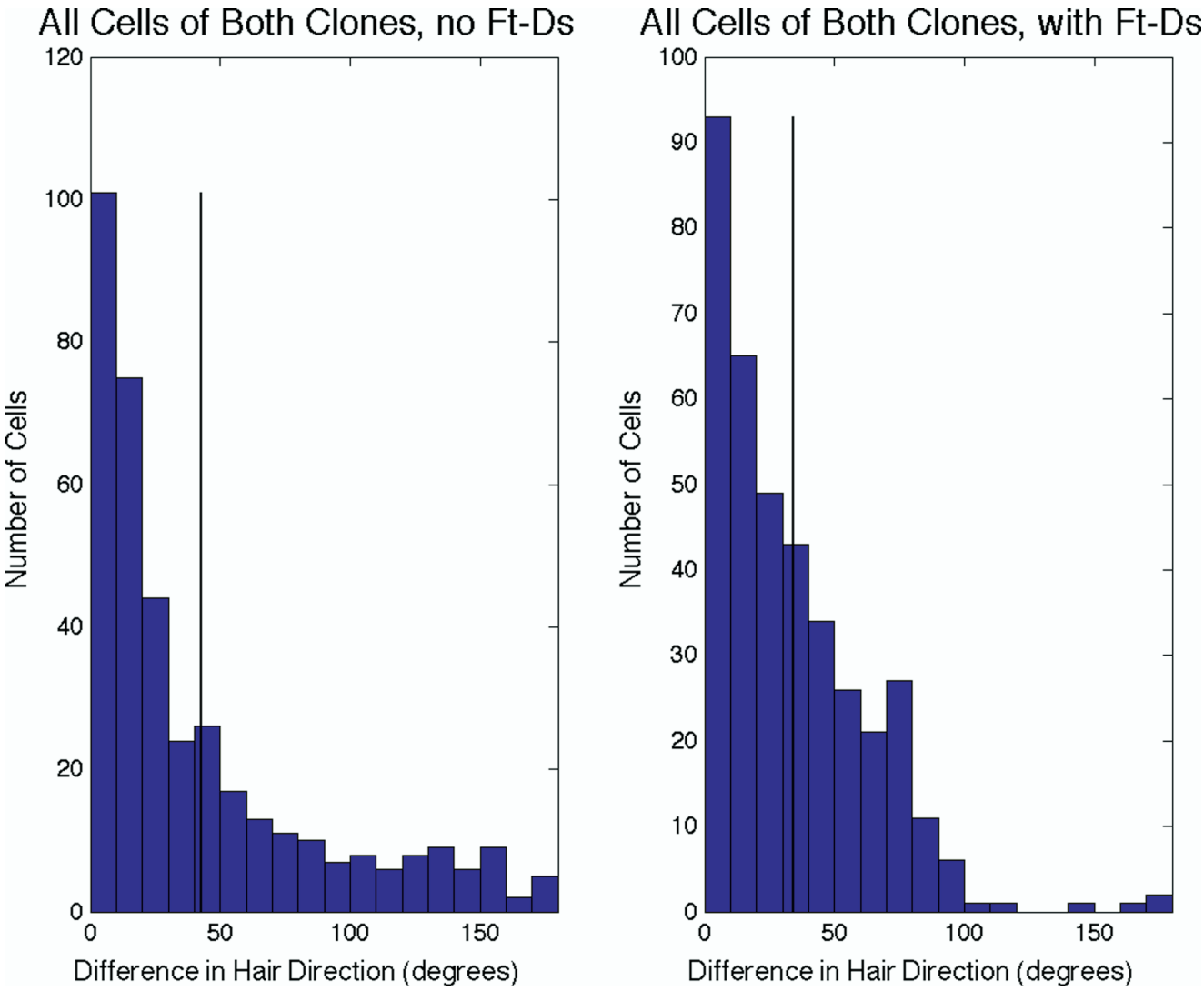

Fig. S7. Two histograms depicting the distribution of the normalized difference in hair direction for both clones, in the no Ft-Ds case (*Left*) and in the case with the addition of Ft-Ds (*Right*). The width of the bars in the histograms is 10°. The corresponding global averages are also shown.

Table S1. Identified parameters for the mathematical model incorporating irregular cell geometry

Parameter	Value	Parameter	Value	Parameter	Value
$[Dsh]_0$	1.0	R_6	8.34×10^{-1}	λ_6	8.90×10^{-7}
$[Pk]_0$	3.92×10^{-1}	R_7	7.79×10^{-1}	λ_7	2.73×10^{-2}
$[Vang]_0$	1.66	R_8	3.10×102	λ_8	2.12×10^{-3}
$[Fz]_0$	4.82	R_9	1.90×105	λ_9	3.36
M	9.26×10^{-1}	R_{10}	2.23×103	λ_{10}	2.33×10^{-6}
R_1	7.70	λ_1	2.13×10	K_b	1.64×10
R_2	1.36×10	λ_2	8.15×105	K_p	2.36
R_3	8.69×10	λ_3	5.98×10^{-2}	M_{lC}	5.68×10^{-1}
R_4	2.41	λ_4	2.77×10^{-3}	M_o	5.77
R_5	4.78×10^{-6}	λ_5	8.82×10^{-8}	M_{bcl}	1.26

Other Supporting Information Files

SI Appendix